NASA

Technical Memorandum 83899

# Charged Particle Motions in the Distended Magnetospheres of Jupiter and Saturn

**Thomas J. Birmingham**



**FEBRUARY 1982**



National Aeronautics and
Space Administration

**Goddard Space Flight Center**
Greenbelt, Maryland 20771

# CHARGED PARTICLE MOTIONS IN THE DISTENDED MAGNETOSPHERES OF JUPITER AND SATURN

Thomas J. Birmingham
Planetary Magnetospheres Branch
Laboratory for Extraterrestrial Physics
NASA/Goddard Space Flight Center
Greenbelt, Maryland 20771

## ABSTRACT

Charged particle motion in the guiding center approximation is analyzed for models of the Jovian and Saturnian magnetospheric magnetic fields based on Voyager magnetometer observations. Field lines are traced and shown to exhibit the previously recognized [Connerney et al., 1981a,b] distention which arises from azimuthally circulating magnetospheric currents. The spatial dependencies of the guiding center bounce period and azimuthal drift rate are investigated for the model fields. The bounce period may be shorter or longer by a factor of 1-3 than in the field of the planetary dipole alone depending on whether a particle mirrors close to the magnetic equator and experiences predominantly an enhanced mirror force or at high latitude and is affected principally by the extended length of the field line. Non-dipolar effects in the gradient-curvature drift rate are most important at the equator and affect particles with all mirror latitudes. The effect is a factor of 10-15 for Jupiter with its strong magnetodisc current and 1-2 for Saturn with its more moderate ring current. Limits of adiabaticity, where particle gyroradii become comparable with magnetic scale lengths, are discussed and are shown to occur at quite modest kinetic energies for protons and heavier ions.


## INTRODUCTION

Owing to the rapid rotation rates of Jupiter and Saturn and the large radial extents of their magnetospheres, diamagnetic currents carried by magnetospheric plasma rotating azimuthally around the planets contribute significantly to the magnetospheric magnetic fields. This effect is especially important for Jupiter with its stronger internal field and hence larger magnetosphere. It is an effect imbedded in pre-encounter ideas [Hines, 1964; Gledhill, 1967; Piddington, 1969; Ioannidis and Brice, 1971], confirmed by the first Pioneer magnetometer measurements at Jupiter in 1973 [Smith et al., 1974] and Saturn in 1979 [Smith et al., 1980], and incorporated immediately into post-encounter Jovian models [Barish and Smith, 1975; Beard and Jackson, 1976; Gleeson and Axford, 1976; Goertz et al., 1976]. The Voyager 1 and 2 missions in 1979 and 1981 have expanded enormously our knowledge of the Jovian and Saturnian magnetospheres.

In this paper we use planetary magnetic field and magnetodisc ring current models developed to fit Voyager vector magnetometer observations [Ness et al., 1979a, b; 1981] to compute guiding center bounce periods and gradient-curvature drift speeds in the Jovian and Saturnian magnetospheres. We find that magnetic field components arising from azimuthal plasma currents have a substantial effect on drifts, which for Jupiter are a factor of 10 or more larger than in a simple dipole approximation. Such drift corrections must be taken into account in calculating anisotropies of >100 keV electrons and ions in the middle magnetospheres of both planets. They also appear to be significant for calculating absorption lifetimes by the moons Ganymede (Jupiter) and Rhea (Saturn) and they should be dramatically important at Callisto (Jupiter), although there is no reported particle absorption there.

Our interest is with magnetically trapped ions and electrons, adiabatic in the usual sense that the ratio $\epsilon = r_G/L$ of their gyroradii $r_G$ to the scale length L of the magnetic field is small and energetic in the sense that $\underset{\sim}{E}\times\underset{\sim}{B}$ drift speeds $u_E$ are of $\theta(\epsilon)$ compared with thermal speeds v. We are thus concerned with the situation where $\underset{\sim}{E}\times\underset{\sim}{B}$, gradient, and curvature drifts are of the same order in $\epsilon$.

## MAGNETIC MODELS

We use topologically similar current sheet magnetic models which have been developed to fit Voyager observations at Jupiter [Connerney et al., 1981a] and Saturn [Connerney et al., 1981b]. In each instance the magnetic field consists of a contribution arising from processes internal to the planet plus the field of a current flowing azimuthally in a planet-centered cylindrical coordinate system with its z-axis aligned with the planetary dipole. In such coordinates the model magnetic fields are both azimuthally symmetric and north-south symmetric (i.e., with respect to the z = 0 plane). Magnetic field lines lie entirely in meridional planes (They have only $B_\rho$, $B_z$ components.), the observed $B_\phi$ sweepback being an effect soon to be incorporated into such models [Connerney et al., 1982]. The plasma current flows in a clockwise direction, when viewing along the z-axis, which is also the direction of corotation when the dipole and planetary rotation axes are aligned, as they essentially are in the case of Saturn.

The z' integral can also be done. The resultant expression is lengthy, so we adopt the following convenient notation

$$z_{\pm} = z \pm D$$

$$\alpha_{o,1} = R_{o,1} - \rho\cos\phi'$$

$$\beta_{o,1} = R_{o,1}^2 - 2\rho R_{o,1}\cos\phi' + \rho^2 = \alpha_{o,1}^2 + \rho^2\sin^2\phi'$$

$$S_{o,1}^{+,-} = (z_{+,-}^2 + \beta_{o,1})^{1/2} + \alpha_{o,1}$$

Because of the z-symmetry we limit ourselves to $z \geq 0$ and obtain

$$A_\rho = \frac{-\mu_o I_o}{2\pi}\int_0^\pi d\phi'\ \cos\phi'\ \{\alpha_o \ln(z^+ + S_o^+ - \alpha_o) - \alpha_1 \ln(z^+ + S_1^+ - \alpha_1) + z^+ \ln(S_o^+/S_1^+)$$

$$- \rho\sin\phi'\ [\sin^{-1}\left(\frac{\alpha_o S_o^+ + \rho^2\sin^2\phi'}{S_o\sqrt{\beta_o}}\right) - \sin^{-1}\left(\frac{\alpha_1 S_1^+ + \rho^2\sin^2\phi'}{S_1\sqrt{\beta_1}}\right)]$$

$$+ (\alpha_1 \ln\beta_1 - \alpha_o \ln\beta_o)/2\ \} - (-1)^H(z^+ + |z^-|) \qquad (4)$$

Here H(D-z) is the step function

$$H = 1 \qquad z < D$$

$$= 0 \qquad z \geq D$$

$(-1)^H (z^+ + |z^-|)$ indicates a term, identical to the entire preceding expression with $z^+$ replaced by $|z^-|$ (so that $S_o^+$ and $S_1^+$ are also replaced by $S_o^-$ and $S_1^-$) and having an algebraic sign determined by the sign of z-D. The remaining $\phi'$ integral is then carried out numerically.

At the radial distances of interest, only the dipole term from the internal field is important. Adding it to the current sheet contribution, we obtain for the field components

$$B_\rho = \frac{3a_o \rho z}{r^5} - \frac{\partial A_p}{\partial z} \tag{5a}$$

$$B_z = \frac{a_o}{r^3}\left(\frac{3z^2}{r^2} - 1\right) + \frac{A_p}{\rho} + \frac{\partial A_p}{\partial \rho} \tag{5b}$$

Since the only appearance of z in Eq. (3) is in the limits of integration, $\partial A_p / \partial z$ is most readily obtained by differentiating this form

$$\frac{\partial A_p}{\partial z} = \frac{\mu_o I_o}{2\pi} \int_o^\pi d\phi' \cos\phi' \ln\left(\frac{S_1^+}{S_o^+}\frac{S_o^-}{S_1^-}\right)$$

On the other hand, no such compact representation of $\partial A_p / \partial \rho$ is apparent. We have therefore evaluated this derivative numerically.

Shown in Fig. 1a as solid curves are Jovian magnetic field lines obtained by integrating the equation

$$\frac{d\rho}{dz} = \frac{B_\rho}{B_z}$$

beginning at equatorial (z=0) points displaced at 5 $R_J$ intervals from the center of the planet. Note the different scales on the vertical and horizontal axes. The 7 dotted curves are dipole field lines which intersect Jupiter's surface at the same latitudes as the 7 distended field lines. In the magnetodisc ($\rho_o$ > 15 $R_J$) the remnant magnetic field at the equator is weak, so that much of this equatorial region maps to a small range of magnetic

latitude around 73° at Jupiter's surface. In identifying accurately the intersection latitudes we have used the fact that for any meridional field $\rho A_\phi$ is constant along field lines. Finally for later use in specifying mirror points of trapped particles, there appears in Fig. 1a a grid of constant magnetic latitude lines.

Figure 1b is the corresponding situation for Saturn's magnetosphere. Field lines are once again distended but to a far lesser degree than for Jupiter's magnetodisc.

Although our methods for calculating the magnetic field differ, the results in Figs. 1 agree with those of Connerney et al. [1981a, 1981b].

## GRADIENT AND CURVATURE DRIFTS

We begin with the well known, relativistically correct expression [Northrop, 1963]

$$\underset{\sim}{\dot{R}}_\perp = \frac{m_o \gamma c}{e} \frac{\hat{e}_1}{B} \times \left( \frac{v_\perp^2}{2B} \underset{\sim}{\nabla} B + v_\parallel^2 \frac{\partial \hat{e}_1}{\partial s} \right) \tag{6}$$

for the $\theta(\epsilon)$ component of the guiding center drift velocity due to spatial inhomogeneity of the magnetic field. Here $\hat{e}_1 = \underset{\sim}{B}/|\underset{\sim}{B}|$, $v_\parallel = \underset{\sim}{v} \cdot \hat{e}_1$, $v_\perp = (v^2 - v_\parallel^2)^{1/2}$, $\partial \hat{e}_1 / \partial s = \hat{e}_1 \cdot \underset{\sim}{\nabla} \hat{e}_1$ is the derivative of $\hat{e}_1$ with respect to distance s along field lines, $\gamma = (1 - v^2/c^2)^{-1/2}$ is the Lorentz factor, and $m_o$ and $e$ are the rest mass and (signed) charge of the drifting particle.

From conservation of magnetic moment M

$$M = \frac{\gamma^2 m_o v_\perp^2}{2B(s)} = \text{const.}$$

we obtain

$$\gamma v_\perp^2 = \frac{2MB}{\gamma m_o} \tag{7}$$

and

$$\gamma v_{\parallel}^{\ 2} = \gamma v^2 - \frac{2MB}{\gamma m_o} = \frac{\gamma^2-1}{\gamma} c^2 - \frac{2MB}{\gamma m_o} \tag{8}$$

Furthermore it is shown readily that

$$\hat{e}_1 \times \frac{\partial \hat{e}_1}{\partial s} = \frac{1}{B} (\nabla \times \underset{\sim}{B})_\perp + \frac{\underset{\sim}{B} \times \nabla B}{B^2} \tag{9}$$

$$= \frac{\mu_o \underset{\sim}{I}_\perp}{B} + \frac{\underset{\sim}{B} \times \nabla B}{B^2}$$

where the $\perp$ subscript denotes the vector component perpendicular to $\underset{\sim}{B}$. ($\underset{\sim}{I}$ is totally perpendicular to $\underset{\sim}{B}$ in the models used in this paper.) Using Eqs. (7-9) in Eq. (6) we write

$$\dot{\underset{\sim}{R}}_\perp = \frac{c}{eB^2} \left[ \left( \frac{\gamma^2-1}{\gamma} m_o c^2 - \frac{MB}{\gamma} \right) \frac{\underset{\sim}{B} \times \nabla B}{B} + \left( \frac{\gamma^2-1}{\gamma} m_o c^2 - \frac{2MB}{\gamma} \right) \mu_o \underset{\sim}{I}_\perp \right] \tag{10}$$

Note finally that in terms of the field strength $B_m$ at the mirror points of the bouncing (as well as drifting) guiding centers

$$\frac{MB}{\gamma} = \frac{\gamma m_o v^2}{2} \frac{B}{B_m} = \frac{\gamma^2-1}{\gamma} m_o c^2 \frac{B}{2B_m} \tag{11}$$

and

$$\dot{\underset{\sim}{R}}_\perp = \frac{m_o c^3}{e} \frac{\gamma^2-1}{\gamma} \frac{1}{B^2} \left[ \left( 1 - \frac{B}{2B_m} \right) \frac{\underset{\sim}{B} \times \nabla B}{B} + \left( 1 - \frac{B}{B_m} \right) \mu_o \underset{\sim}{I}_\perp \right] \tag{12}$$

Thus the energy dependence is a strictly multiplicative factor, while spatial and pitch angle dependencies, the latter entering through $B_m$, are in general intertwined in a complicated way.

Like the current density $\underset{\sim}{I}$ (cf. Eq. 1), $\underset{\sim}{B}\times\underset{\sim}{\nabla}B$ is totally azimuthal

$$\underset{\sim}{B}\times\underset{\sim}{\nabla}B = \hat{e}_\phi \left[\frac{B_z}{B}\left(B_\rho \frac{\partial B_\rho}{\partial \rho} + B_z \frac{\partial B_z}{\partial \rho}\right) - \frac{B_\rho}{B}\left(B_\rho \frac{\partial B_\rho}{\partial z} + B_z \frac{\partial B_z}{\partial z}\right)\right] \tag{13}$$

so that $\dot{\underset{\sim}{R}}_\perp$ is in the $\pm\,\hat{e}_\phi$ direction. For computational convenience we eliminate $\partial B_z/\partial z$ and $\partial B_z/\partial \rho$ by using Maxwell's Equations $\underset{\sim}{\nabla}\cdot\underset{\sim}{B} = 0$

$$\frac{\partial B_z}{\partial z} = -\frac{B_\rho}{\rho} - \frac{\partial B_\rho}{\partial \rho} \tag{14}$$

and $\underset{\sim}{\nabla} \times \underset{\sim}{B} = \mu_o \underset{\sim}{I}$

$$\frac{\partial B_z}{\partial \rho} = \frac{\partial B_\rho}{\partial z} - \mu_o I \tag{15}$$

Using Eqs. (13-15) we finally express $\dot{\underset{\sim}{R}}_\perp$ as

$$\dot{\underset{\sim}{R}}_\perp = \frac{m_o c^3}{e} \frac{\gamma^2-1}{\gamma} \frac{1}{B^4} \hat{e}_\phi$$

$$\left\{\left[-\frac{B_\rho^2 B_z}{\rho} + 2B_\rho B_z\left(\frac{B_\rho}{\rho} + \frac{\partial B_\rho}{\partial \rho}\right) + \left(B_z^2 - B_\rho^2\right)\frac{\partial B_\rho}{\partial z} + \mu_o I\, B_\rho^2\right]\right.$$

$$- \frac{B}{2B_m}\left[- \frac{B_\rho^2 B_z}{\rho} + 2B_\rho B_z\left(\frac{B_\rho}{\rho} + \frac{\partial B_\rho}{\partial \rho}\right) + \left(B_z^2 - B_\rho^2\right)\frac{\partial B_\rho}{\partial z} + \mu_o I\left(2B_\rho^2 + B_z^2\right)\right]\right) \quad (16)$$

Here we have separated terms which depend on pitch angle through $B_m$ from those which do not.

A useful measure of the azimuthal drift rate is the angular velocity $\dot{\omega} = \dot{R}_\perp/\rho$, where $\dot{\omega}$ is a signed quantity, positive in the direction of increasing $\phi$. $\dot{\omega}$ varies on the rapid time scale of the guiding center bounce motion both because of its dependence on $\rho$, which varies with position along field lines, and the dependence of $\dot{R}_\perp$ on $B$, its derivatives, and I along the bounce path. This rapid time variation can be removed by averaging $\dot{\omega}$ over the bounce. We denote this bounce average by $\langle \dot{\omega} \rangle$

$$\langle \dot{\omega} \rangle = \frac{1}{\tau_B} \oint \frac{ds}{v_\parallel} \dot{\omega} = \frac{1}{\tau_B} \oint \frac{ds}{v_\parallel} \frac{\dot{R}_\perp}{\rho} \quad (17)$$

Here the $v_\parallel^{-1}$ factor accounts for the varying amounts of time spent at different points s along the field line, the integral extends over a complete bounce path to and fro between each mirror point, and the bounce period $\tau_B$ is the usual

$$\tau_B = \oint \frac{ds}{v_\parallel} \quad (18)$$

Because of the north-south symmetry assumed here, the integrals in Eqs. (17) and (18) each reduce to 4 times the integral from the equator, which we take to be the s = 0 surface, to the northern mirror point, denoted by $s_m$. Furthermore by Eqs. (8) and (11) we can relate $v_\parallel(s)$ to B(s), $B_m$, and the magnetic moment M which is a constant of the bounce motion

$$v_{\parallel} = \left(\frac{2MB_m}{\gamma^2 m_o}\right)^{1/2} \left(1 - \frac{B}{B_m}\right)^{1/2} = v\left(1 - \frac{B}{B_m}\right)^{1/2}$$

so that

$$\tau_B = \frac{4}{v} \int_o^{s_m} \frac{ds}{\left(1 - \frac{B}{B_m}\right)^{1/2}} \tag{19}$$

and

$$\langle \dot{\omega} \rangle = \frac{\int_o^{s_m} \frac{ds}{\left(1 - \frac{B}{B_m}\right)^{1/2}} \frac{\dot{R}_\perp}{\rho}}{\int_o^{s_m} \frac{ds}{\left(1 - \frac{B}{B_m}\right)^{1/2}}} \tag{20}$$

where, by definition, $B(s_m) = B_m$.

For comparison of our result here with dipole results [Hamlin et al., 1961; Lew, 1961; Thomsen and Van Allen, 1981] we define

$$H_{J,S} = \frac{1}{LR_{J,S}} \int_o^{s_m} \frac{ds}{\left(1 - \frac{B}{B_m}\right)^{1/2}} \tag{21}$$

so that

$$\tau_B = \frac{4}{v} L R_{J,S} H \tag{22}$$

Here

$$L = \frac{(z_m^2 + \rho_m^2)^{3/2}}{\rho_m^2} \tag{23}$$

is the equatorial crossing distance in planetary radii $R_J$ or $R_S$ of the dipole field line which would pass through the mirror point, whose coordinates are $\rho_m$, $z_m$. It is easily shown that for any dipole field H, as defined by Eq. (21), is independent of L and depends only on mirror latitude $\lambda_m$. Thus for a dipole field H is independent of position along the lines of constant magnetic latitude shown in Figs. 1.

Such is not the case when the magnetic fields arising from plasma currents are added. We have evaluated $H(\rho_o, \lambda_m)$ by numerically integrating Eq. (21) using the model field for particle motion along field lines intersecting the equator at different distances $\rho_o$ and also for different values of mirror latitude $\lambda_m$. Given an observational position and a particle detector look direction, $\rho_o$ can be estimated from Figs. 1 and $\lambda_m$ can be determined by magnetic moment conservation. The latter requires magnetic intensity information which is available in the publications of Connerney et al. [1981a,b].

The H values in Figs. 2 corresponding to $\rho_o = 0$ are the L-independent dipole values, since as $\rho_o \to 0$ the magnetic model is dominated by its dipole component. We thus see that for particles mirroring at $\lambda_m \geq 20°$, H and hence $\tau_B$ are larger than they would be in a dipole field for a particle mirroring at the same $\rho_m$, $z_m$. The reason is that the model field line is longer than the corresponding dipole line because of the stretching out of magnetic field lines by the plasma current. This effect is much more important for Jupiter than it is for Saturn, as one would expect by visual inspection of Figs. 1. In Fig. 2b the tapering off of the slope of the 20°-60° contours near $\rho_o = 15$ $R_S$ is a result of the fact that the distention of field lines abates and they become more dipole-like at radial distances beyond the current sheet.

At smaller $\lambda_m$, H generally has a smaller value than it does for a dipole. Here the difference in length between model and dipole field lines becomes secondary to the difference in mirror forces between them. Recall [Roederer, 1970] that a particle mirroring near a point $s_o$ of minimum intensity along a

magnetic field line (i.e., a point where $\partial B/\partial s = 0$) executes simple harmonic motion described by the equation

$$\ddot{s} = -\left[\frac{\partial^2 B/\partial s^2(s_o)}{2B(s_o)}\, v^2\right](s - s_o) \tag{24}$$

about $s_o$. Thus

$$\tau_B = \frac{2\pi}{v}\left[\frac{2B(s_o)}{B''(s_o)}\right]^{1/2}$$

from which we identify

$$H_{J,S} = \frac{\pi}{2}\,\frac{1}{LR_{J,S}}\left(\frac{2B}{B''}\right)^{1/2} \tag{25}$$

For the ranges of $\rho_o$ in Figs. 2 a single intensity minimum occurs on each model field line at the $z = 0$ magnetic equator with the exception of a small region around $\rho_o = 15\ R_S$ near the outer terminus of Saturn's ring current. We shall return shortly to a brief discussion of this anomalous region. For any meridional field with continuous components and having north-south symmetry

$$B''(z=0) = \frac{\partial^2 |B_z|}{\partial z^2} + \frac{1}{B}\frac{\partial B_\rho}{\partial z}\left(\frac{\partial B_\rho}{\partial z} + \frac{\partial B_z}{\partial \rho}\right)$$

$$= \frac{\partial^2 |B_z|}{\partial z^2} + \frac{1}{B}\frac{\partial B_\rho}{\partial z}\left(2\,\frac{\partial B_\rho}{\partial z} - \mu_o I\right) \tag{26}$$

with the right hand side, of course, evaluated at $z = 0$. The curves marked $\lambda_m = 0^\circ$ in Figs. 2 have been constructed using Eqs. (25) and (26). The $\rho_o = 0$, $\lambda_\mu = 0$ dipole value of $H = \pi/(18)^{1/2}$ follows directly. The diminution from this dipole value for $\rho_o > 0$ is due mostly to a large $(\partial B_\rho/\partial z)^2$ term in Eq. (26) which reflects the 'hairpin' character of field lines near the equator, especially in the $\rho_o \geq 15\ R_J$ region of Jupiter's magnetosphere.

An interesting aberration occurs in the $\rho_o \approx 15\ R_S$ near equatorial region of Saturn's magnetosphere. Over a small radial range of perhaps .5 $R_S$ in extent, the point of minimum B bifurcates from the z = 0 plane into the northern and southern magnetic hemispheres. As this region is approached along the equator, B'' diminishes so that an equatorial particle executes slower bounce motion which is manifested by an increasing $H_s$. When the point of minimum B leaves the equator, B'' changes sign, z = 0 is no longer an oscillation point, and $H_s$ no longer has a real value. It is apparent from Fig. 2b that the field minimum departs less than 10° in latitude from the equator, for particles oscillating about the equator can mirror at $\lambda_m = 10°$. Such a non-equatorial trapping geometry was suggested for Jupiter by Barish and Smith [1975]. At $\rho_o = 16\ R_s$, outside the Saturnian ring current, $H_s$ is again finite for all $\lambda_m$, indicating that the point of minimum B is once more at z = 0.

With regard to drifts, let us again establish contact with previous dipole work [Hamlin et al., 1961; Lew, 1961; Thomsen and Van Allen, 1981] by defining (cf. Eqs. (16) and (20))

$$\langle \dot{\omega} \rangle = \frac{3}{2}\frac{m_o c^3}{eR_{J,S}^2}\frac{\gamma^2-1}{\gamma}\frac{L}{B_{J,S}}\left(\frac{F}{G}\right)_{J,S} \qquad (27)$$

Here $B_{J,S}$ is the magnitude of the dipole field at the planetary equator (4 G for Jupiter; .209 G for Saturn) and L is as previously defined in Eq. (23). Thus

$$\left(\frac{F}{G}\right)_{J,s} = \left(\frac{3}{2}\frac{m_o c^3}{eR_{J,S}^2}\frac{\gamma^2-1}{\gamma}\frac{L}{B_{J,S}}\right)^{-1}\frac{\int_o^{s_m} ds\,\frac{1}{\left(1-\frac{B}{B_m}\right)^{1/2}}\,\frac{\dot{R}_\perp}{\rho}}{\int_o^{Sm} ds\,\frac{1}{\left(1-\frac{B}{B_m}\right)^{1/2}}} \qquad (28)$$

with F/G independent of particle species and energy. In general F/G is a function of $\lambda_m$ and $\rho_o$, but in the case of a pure dipole field its $\rho_o$ ($\equiv$ L) dependence vanishes, and, like H previously, F/G becomes a function of $g_m$ alone.

Figures 3a and 3b show F/G for the Jovian and Saturnian models respectively in the same format used in Figs. 2. The L-independent dipole values are again the limiting forms as $\rho_o \to 0$ and the magnetospheric current becomes a negligible factor.

For both magnetospheres the most significant deviation from the dipole results is for equatorially mirroring ($\lambda_m = 0$ particles). For such particles Eq. (28) becomes

$$\left(\frac{F}{G}\right)_{J,S}(\lambda_m = 0,\ \rho_o) = \left(\frac{3}{2}\frac{\bar{m}_o c^3}{eR_{J,S}^2}\frac{\gamma^2-1}{\gamma}\frac{\rho_o}{B_{J,S}}\right)^{-1}\frac{\dot{R}_\perp(z=0)}{\rho_o R_{J,S}}$$

which upon substitution from Eq. (16), noting that $B_\rho(z=0) = 0$, $B_m = B$, and $\rho_o = LR_{J,S}$ becomes

$$\left(\frac{F}{G}\right)_{J,S}(\lambda_m=0,\ \rho_o) = \frac{1}{3}\frac{B_{J,S}R_{J,S}}{L^2B^2}\left(\frac{\partial B_\rho}{\partial z} - \mu_o I\right) = \frac{1}{3}\frac{B_{J,S}R_{J,S}}{L^2B^2}\frac{\partial B_z}{\partial \rho} \qquad (29)$$

(The dipole case where $F/G(\lambda_m=0) = 1$ follows immediately from Eq. 29.) The $\lambda_m = 0°$ curves in Figs. 3 are plotted using Eq. 29.

For Jupiter the deviation from the dipole result is an order of magnitude or more near $\rho_o = 25\ R_J$. The enhancement is a consequence of the $B^{-2}$ factor in Eq. (29) and the very weak field at the center of the current sheet. In

fact the magnetic field is so weak and changes so rapidly due to the strong $\partial B_\rho/\partial z$ that one should worry about the smallness of $\epsilon$ and the validity of the adiabatic approximation. Knowing that one can go to low enough particle energy that $\epsilon$ is small, we shall proceed here and return in the next section to quantify this limitation.

We have evaluated F/G numerically and found for Jupiter very little dependence on $\lambda_m$ at given $\rho_o$ over the range $10^\circ \leq \lambda_m \lesssim 60^\circ$. Hence we have drawn in Fig. 3a only two of the closely nested curves in this $\lambda_m$ interval. The reason is that the numerator integral in Eq. 28

$$\int_0^{S_m} ds \frac{1}{\left(1 - \frac{B}{B_m}\right)^{1/2}} \frac{\dot{R}_\perp}{\rho}$$

picks up a large (almost its entire) contribution from the z = 0 region where B is small: a particle may mirror far from the equator but the major contribution to its drift motion occurs in that brief interval during which it passes through the equator. The denominator integral

$$\int_0^{S_m} ds \frac{1}{\left(1 - \frac{B}{B_m}\right)^{1/2}} = LR_J H_J$$

on the other hand has contributions from all s values, with a sizable amount coming from the region about the mirror point. Thus $LR_J H_J$ increases with $\lambda_m$ at fixed $\rho_o$ as the particle traversal distance increases. However, in a nearly compensating fashion L decreases with $\lambda_m$ (at fixed $\rho_o$) so that $L^2 H_J$ is approximately constant.

Note finally that $(F/G)_J$ reverses sign for $\lambda_m = 0$ particles in the region $\rho_o > 30\ R_J$: the sense of the gradient drift changes from generally prograde

(with respect to the direction of planetary rotation) to retrograde, or vice versa, depending on the sign of the electrical charge on a particle. This reversal results from a shift in the algebraic sign of $\partial B_z/\partial\rho(z = 0)$. It is an effect which is confined to the equator and is no longer seen in $(F/G)_J$ ($\lambda_m = 10^\circ$, $\rho_o$): other effects taking place closely off $z = 0$ and which are also important because of weak B soon dominate.

For Saturn the magnetic field at the z=0 center of the ring current is, relative to the field at higher latitudes, nowhere near as weak as at Jupiter. Hence equatorial drifts, while important, are not of sole significance. Rather than being an order of magnitude larger than dipole, $(F/G)_S$ is more usually a factor of 2 greater. What is evident in Fig. 3b and is not apparent in Fig. 3a are discontinuities in F/G at the inner and outer edges of the ring current. These discontinuities result, cf. Eq. (29), from discontinuities in $\partial B_z/\partial\rho$ as $I(\rho)$, cf. Eq. (15), turns on and off at $\rho_o = 8.5\ R_S$ and $15.5\ R_S$ respectively. A discontinuity is also present at $\rho_o = 5\ R_J$ in Fig. 3a, but its evidence is masked by the dominance of the continuous $\partial B_z/\partial\rho$ arising from the Jovian dipole. The discontinuity is evident to a lesser extent at Saturn for $\lambda_m = 10^\circ$, but it clearly has disappeared by the time $\lambda_m = 30^\circ$ is reached.

Were the current distribution $I(\rho)$ continuous, these discontinuities would undoubtedly disappear. However, we expect the qualitative character of $(F/G)_S$ would be preserved, so long as significant $\partial I/\partial\rho$ is concentrated near $8.5\ R_S$ and $15.5\ R_S$.

Note finally the gap in the $\lambda_m = 0^\circ$ curve for $15\ R_S \lesssim \rho_o \lesssim 15.5\ R_S$. Although Eq. (28) yields a real value for $(F/G)_S$ in this interval, we know from our bounce time discussion that $z = 0$ is no longer a stable oscillation point: the canceling numerator and denominator integrals in Eq. (28) for z=0 particles are in this instance both imaginary.

## DISCUSSION

Weak B(z=0) means that particles have large gyro-radii at the equator. Large $\partial B_\rho/\partial z$ (z=0) means a short scale length L for the magnetic field. The adiabatic approximation and our results are hence suspect, particularly for

Jupiter. As a measure of the range of validity of the adiabatic approximation we have determined the value of particle kinetic energy K for which $\epsilon = 1$ at $z = 0$. This value depends on $\lambda_m$, for particles mirroring high off the equator pass through it with shallow pitch angles and consequent small gyro-radii compared with particles of the same energy which are mirroring at the equator.

If we take L to be $B(z=0)/\partial B_\rho/\partial z(z=0)$ it is straightforward to show that the $\epsilon = 1$ condition leads to the following equation for $K = (\gamma-1)m_o c^2$

$$\frac{K}{m_o c^2} = \{1 + [\frac{3\times10^{-4}\,\mathfrak{z}\,B^2(z=0)}{m_o c^2\ \partial B_\rho/\partial z(z=0)}\ \frac{1}{\sin\theta_e}]^2\}^{1/2} - 1 \qquad (30)$$

Here $\mathfrak{z}$ is the ionization state of the particle (+1 for protons, -1 for electrons etc.) and $m_o c^2$ its rest energy in MeV. Particles with kinetic energy lower than that given by Eq. (30) have gyro-radii smaller than L, and hence this K is the upper energy limit for adiabaticity. In Fig. 4a we have plotted the characteristic factor $K_c = 3\times10^{-4}\ B^2(z=0)/\partial B_\rho/\partial z(z=0)$ for that portion of the Jovian magnetosphere where adiabaticity is suspect.

Note that this quantity is always at least an order of magnitude larger than $m_o c^2 = .511$ MeV for electrons, so that $K_e = K_c/\sin\theta_e$ is at least 5 MeV in magnitude. We thus conclude that electrons up to approximately 5 MeV are adiabatic and have been treated validly in this paper. The limit is in fact considerably higher for electrons with larger $\lambda_m$ because of the $(\sin\theta_e)^{-1}$ factor in Eq. (30).

The case is, however, different for protons and heavier ions. Shown also in Fig. (4a) are solutions to Eq. (29) for protons with 3 different values of $\sin\theta_e$. Values of $\sin\theta_e = .05$ and .01 correspond roughly to particles mirroring at $\lambda_m = 30°$ and $\lambda_m = 60°$ in this $\rho_o$ region of the Jovian magnetosphere. Note that the adiabaticity condition is quite severe for equatorial protons, with $K_p(\sin\theta_e = 1)$ being as small as 15 keV. However, for protons mirroring at higher latitudes $K_p$ is greater than 600 keV.

For heavier ions and for all but the smallest $\sin\theta_e$, we can expand the square root in Eq. (30) according to $(1+\epsilon^2)^{1/2} \approx 1 + \epsilon^2/2$ and obtain

$$K_i = \frac{z^2}{2m_o c^2 \sin^2\theta_e} K_c^2$$

For $S^+$ with $\sin\theta_e = .05$, $K_i$ is 167 keV at $\rho_o = 29\ R_J$, and thus a sizable portion of the sulfur ions in Jupiter's magnetosphere may be non-adiabatic.

Figure 4b shows the corresponding situation for Saturn. Note that because Saturn's field lines are far less distended than Jupiter's, $\partial B_\rho/\partial z(z=0)$ is much smaller, and the maximum energy for which particles are adiabatic correspondingly higher. All electrons below 300 MeV are at least marginally adiabatic. The 3 proton curves correspond once again to particles mirroring at the equator ($\sin\theta_e=1$) and at approximately 30°($\sin\theta_e = .4$) and 60°($\sin\theta_e = .05$) magnetic latitude near $\rho_o = 12\ R_S$.

In Figures 5 we plot for each magnetosphere the value of $K_e$ for which $\langle\dot{\omega}\rangle$ is equal in magnitude to the planetary angular rotation frequency $\Omega_{J,S}$($2\pi/\Omega_J = 10$ hrs., $2\pi/\Omega_S = 10.7$ hrs.). Recall that $\langle\dot{\omega}\rangle$ depends on the sign of particle charge and is retrograde with respect to planetary rotation for electrons and prograde for protons, expect for equatorially mirroring ($\lambda_m=0°$) particles in the $\rho_o > 30\ R_J$ and $14\ R_S < \rho_o < 15\ R_S$ regions where $\partial B_z/\partial\rho$ switches sign (cf. Eq. 29) and the reverse is true for both species. If we neglect the nonalignment of Jupiter's dipole and rotation axes, the values in Fig. 5 are thus in general those at which an electron has no drift motion in a non-rotating coordinate system: $\langle\dot{\omega}\rangle$ just balances the $\vec{E}\times\vec{B}$ motion which drives particles to co-rotation. Corresponding values of $K_p$ have not been plotted but are approximately 1/2 to 3/4 as large as $K_e$, depending on the value of $\rho_o$.

With the exception of those equatorial regions where $\partial B_z/\partial\rho$ is small so that compensatingly high particle kinetic energy is needed to produce significant gradient-curvature drifts, the values of $K_e$ in Figs. 5 are well within the range of validity of adiabatic theory. On the other hand, the situation is different for protons: values of $K_p$ scaled from Figs. 5 are of

the order of, and in the case of equatorial protons less than, the limits displayed in Figs. 4.

## CONCLUSIONS

The adiabatic motions of charged particles in the distended Jovian and Saturnian magnetospheres are qualitatively similar to those in a dipole field but are quantitatively quite different. Guiding center bounce times may be shorter or longer depending on a particle's mirror latitude: particles mirroring near the magnetic equator experience a stronger-than-dipole mirror force and hence bounce more rapidly than in a dipole field; on the other hand, particles mirroring far from the equator bounce along field lines whose length is significantly enhanced by the distention, and hence such particles have bounce times longer than if they mirrored at the same spatial location in a dipole field. For Jupiter's magnetosphere non-diplar effects on the bounce time are important for radial distances ranging from 10 $R_J$ to 35 $R_J$, the largest distance we have considered, and they vary by a factor of roughly 3 from dipole results. For Saturn the ring current affects the bounce over the 8 $R_S$-16 $R_S$ region, but owing to its weakness relative to Jupiter's magnetodisc current the dipole correction factor is no more than 1.2 - 2.

The bounce-averaged angular drift rate is significantly affected by the field distention. This is so even for particles mirroring at high latitudes where the distention is small: much of their azimuthal drift takes place, especially in the case of Jupiter, during passage through the magnetic equator. In the case of Jupiter the angular gradient-curvature drift is as much as 10-15 times the dipole value and is of most importance between 20 $R_J$ and 35 $R_J$. For Saturn the correction is more nearly a factor of 2 and is of most importance near the inner and outer edges of the ring current at 8.5 $R_S$ and 15.5 $R_S$.

The direction of the gradient-curvature drifts is generally that of co-rotation for protons and in the opposite sense for electrons -- the same as it is for the planetary dipole. In the middle magnetosphere of each planet the magnitude of the gradient-curvature drift in the model field is approximately equal in magnitude to the co-rotation speed for electrons and protons in the 100 keV - 1 MeV range.

Corrections which we have evaluated are thus important in assessing the anisotropies of 100 keV and higher energy particles and should also be accounted for in calculating losses to moons orbiting through the middle magnetospheres. In the case of Jupiter, absorption by Callisto at $\sim$ 27 $R_J$ would be modified significantly by our results. However, no absorption signatures of this moon have been reported from either the Pioneer or Voyager particle experiments. At the orbit of Ganymede near 15 $R_J$, where absorption has been seen [Burlaga et al., 1980] along with signatures of a radially distended magnetic field [Connerney et al., 1981a], we have found the non-dipolar correction to be as large as a factor of 2.5 for equatorial particles and it should be incorporated into a quantitatively accurate analysis. For moons and rings of Jupiter lying within 14 $R_J$ of the planetary surface, effects of the magnetodisc lie mostly in modification of the bounce period (cf. Fig. 2a) for equatorial and near equatorial particles.

In the case of Saturn, Rhea at 8.8 $R_S$ lies in a region where significant non-dipolar effects occur. The deviation of Rhea's absorption as observed in the Voyager 1 cosmic ray experiment [Vogt et al., 1981] from its expected dipole position has been explained successfully using the ring current model [Connerney et al., 1981b]. This suggests that the correction factors which we have calculated and which are most important in this radial region should be applied to any quantitative lifetime calculations.

Finally we mention that because of the diminished scale length of the magnetic field near the equator, protons and heavier ions become non-adiabatic at energies above a few hundred keV. This energy particle appears to dominate the particle energy density of the Jovian middle magnetosphere [Krimigis et al., 1981] and may via its non-adiabatic meandering motion [Sonnerup, 1971] across the field reversal sheet contribute significantly to the magnetodisc current.

Acknowledgments

I thank J. E. P. Connerney for discussions on the topic of the Jovian and Saturnian current sheet and N. F. Ness for reading the manuscript and commenting.

## REFERENCES

Barish, F. D. and R. A. Smith, An analytical model of the Jovian magnetosphere, Geophys. Res. Lett., 2, 269, 1975.

Beard, D. B. and D. J. Jackson, The Jovian magnetic field and magnetosphere shape, J. Geophys. Res., 81, 3399, 1976.

Burlaga, L. F., J. W. Belcher, and N. F. Ness, Disturbances observed near Ganymede by Voyager 2, Geophys. Res. Lett., 7, 21, 1980.

Connerney, J. E. P., M. H. Acuña, and N. F. Ness, Modeling the Jovian current sheet and inner magnetosphere, J. Geophys. Res., 86, 8370, 1981a.

Connerney, J. E. P., M. H. Acuña, and N. F. Ness, Saturn's ring current and inner magnetosphere, Nature, 292, 724, 1981b.

Connerney, J. E. P., M. H. Acuña, and N. F. Ness, Voyager 1 assessment of Jupiter's planetary magnetic field, submitted to J. Geophys. Res.

Gledhill, J. A., Magnetosphere of Jupiter, Nature, 214, 155, 1967.

Gleeson, L. J., and W. I. Axford, An analytical model illustrating the effects of rotation on a magnetosphere containing low energy plasma, J. Geophys. Res., 81, 3403, 1976.

Goertz, C. K., D. E. Jones, B. A. Randall, E. J. Smith, and M. F. Thomsen, Evidence for open field lines in Jupiter's magnetosphere, J. Geophys. Res., 81, 3393, 1976.

Hamlin, D. A., R. Karplus, R. C. Vik, and K. M. Watson, Mirror and azimuthal drift frequencies for geomagnetically trapped particles, J. Geophys. Res., 66, 1, 1961.

Hines, C. O., Hydromagnetic motions in the magnetosphere, Space Sci. Rev., 3, 342, 1964.

Ioannidis, G., and N. Brice, Plasma densities in the Jovian magnetosphere: Plasma sling-shot or Maxwell demon? Icarus, 14, 360, 1971.

Krimigis, S. M., J. F. Carbary, E. P. Keath, C. O. Bostrom, W. I. Axford, G. Gloeckler, L. J. Lanzerotti, and T. P. Armstrong, Characteristics of hot plasma in the Jovian magnetosphere: Results from the Voyager spacecraft, J. Geophys. Res., 86, 8227, 1981.

Lew, J. S., Drift rate in a dipole field, J. Geophys. Res., 66, 2681, 1961.

Ness, N. F., M. H. Acuña, R. P. Lepping, L. F. Burlaga, K. W. Behannon, and F. M. Neubauer, Magnetic field studies at Jupiter by Voyager 1: Preliminary results, Science, 204, 982, 1979a.

Ness, N. F., M. H. Acuña, R. P. Lepping, L. F. Burlaga, K. W. Behannon, and F. M. Neubauer, Magnetic field studies at Jupiter by Voyager 2: Preliminary results, Science, 206, 966, 1979b.

Ness, N. F., M. H. Acuña, R. P. Lepping, J. E. P. Connerney, K. W. Behannon, L. F. Burlaga, and F. M. Neubauer, Magnetic field studies by Voayger 1: Preliminary results at Saturn, Science, 212, 211, 1981.

Northrop, T. G., The Adiabatic Motion of Charged Particles, p. 29, Interscience, New York, 1963.

Panofsky, W. K. H., and M. Phillips, Classical Electricity and Magnetism, p. 117, Addison-Wesley, Reading, 1955.

Piddington, J. H., Cosmic Electrodynamics, Wiley-Interscience, New York, p. 199, 1969.

Roederer, J. G., Dynamics of Geomagnetically Trapped Radiation, p. 37, Springer-Verlag, New York, 1970.

Smith, E. J., L. Davis, Jr., D. E. Jones, P. J. Coleman, Jr., D. S. Colburn, P. Dyal, and C. P. Sonett, Magnetic field of Jupiter and its interaction with the solar wind, Science, 183, 305, 1974.

Smith, E. J., L. Davis, Jr., D. E. Jones, P. J. Coleman, D. S. Colburn, P. Dyal, and C. P. Sonett, Saturn's magnetic field and magnetosphere, Science, 207, 407, 1980.

Sonnerup, B. U. O., Adiabatic particle orbits in a magnetic null sheet, J. Geophys. Res., 76, 8211, 1971.

Thomsen, M. F., and J. A. Van Allen, Motion of trapped electrons and protons in Saturn's inner magnetosphere, J. Geophys. Res., 85, 5831, 1980.

Vogt, R. E., D. L. Chenette, A. C. Cummings, T. L. Garrard, E. C. Stone, A. W. Schardt, J. H. Trainor, N. Lal, and F. B. McDonald, Energetic charged particles in Saturn's magnetosphere: Voyager 1 results, Science, 212, 231, 1981.

TABLE 1. Parameters of the Voyager Middle Magnetosphere Magnetic Models

| | Jupiter | Saturn |
|---|---|---|
| $a_o$ | $4\ G\ R_J^3$ | $.209\ G\ R_S^3$ |
| $\mu_o I_o$ | $4.5 \times 10^{-3}$ G | $5 \times 10^{-4}$ G |
| $R_o$ | $5\ R_J$ | $8.5\ R_S$ |
| $R_1$ | $50\ R_J$ | $15.5\ R_S$ |
| D | $2.5\ R_J$ | $2.5\ R_S$ |

## FIGURE CAPTIONS

Figs. 1. Magnetic field lines in the model Jovian (Fig. 1a) and Saturnian (Fig. 1b) magnetospheres intersecting the equator at several values $\rho_o$. Shown in dotted lines are dipole field lines which intersect the planetary surface at the same latitudes as model field lines (dipole $\rho_o$ labels indicate the correspondence). Note the different scales on the z and $\rho$ axes. Because of strong magnetospheric plasma currents, Jovian field lines can be grossly non-dipolar: much of the Jovian middle magnetosphere maps to a small range of latitudes at the surface of the planet. Lines of constant magnetic latitude are also shown.

Figs. 2. Plots of the bounce period quantity H (cf. Eqs. 21 and 22) for particles in the model Jovian (Fig. 2a) and Saturnian (Fig. 2b) magnetospheres. H depends on the equatorial crossing distance $\rho_o$ of a field line and the particle's mirror latitude $\lambda_m$ on that field line. As $\rho_o \to 0$, H approaches its value in a dipole field, which depends only on $\lambda_m$. For each $\lambda_m$, the ratio $H(\rho_o, \lambda_m)/H(0,\lambda_m)$ is the ratio of the bounce time of a particle mirroring at $\lambda_m$ on a model field line passing through the equator at distance $\rho_o$ to the bounce time of a particle of the same energy mirroring at the same spatial point $(\rho_m, z_m)$ but in the dipole field alone.

Figs. 3. Plots of the azimuthal drift rate quantity F/G (cf. Eqs. 27 and 28) for particles in the model Jovian (Fig. 3a) and Saturnian (Fig. 3b) magnetic fields. F/G depends on the equatorial crossing distance $\rho_o$ of a field line and the particle's mirror latitude $\lambda_m$ on that field line. As $\rho_o \to 0$, F/G approaches its value in a dipole field, which depends only on $\lambda_m$. For each $\lambda_m$, the ratio $F(\rho_o, \lambda_m)\, G(0,\lambda_m)/G(\rho_o, \lambda_m)\, F(0,\lambda_m)$ is the ratio of the longitudinal drift rate of a particle mirroring at $\lambda_m$ on a model field line passing through the equator at distance $\rho_o$ to the longitudinal drift rate of a particle of the same energy mirroring at the same spatial point $(\rho_m, z_m)$ but in the dipole field alone.

Figs. 4. Shown for the model Jovian (Fig. 4a) and Saturnian (Fig. 4b) magnetospheres is the quantity $K_c = 3\times10^{-4} B^2(z=0)/\partial B_\rho/\partial z(z=0)$ which is

characteristic in determining limits of adiabaticity (cf. Eq. 30). Shown also are values of proton kinetic energy as determined from Eq. (30) at which the proton gyro-radius equals the scale length of the field as determined from $B(z=0)/\partial B_\rho/\partial z(z=0)$ for representative values of equatorial pitch angle $\theta_e$. For electrons $K_e$ is always greater tnan $K_c$ and hence the adiabaticity condition is less severe on them, as would be expected on the basis of their smaller mass.

Figs. 5. Shown for the model Jovian (Fig. 5a) and Saturnian (Fig. 5b) magnetospheres is the value $K_e$ of electron kinetic energy at which the longitudinal drift rate $\langle\dot{\omega}\rangle$ equals the planetary angular rotation rate $\Omega_{J,S}$. With limited exceptions, which are discussed in the text, the sense of $\langle\dot{\omega}\rangle$ is prograde for protons and retrograde for electrons. Discontinuities in the Saturnian curves at 8.5 $R_S$ and 15.5 $R_S$ for equatorial particles reflect discontinuities in $\langle\dot{\omega}\rangle$ owing to discontinuities in $\partial B_z/\partial\rho$ which occur at the boundaries of the model current sheet. At $\rho_o \gtrsim 30\ R_J$ and $\rho_o \gtrsim 14\ R_S$, $K_e \to \infty$ for equatorial particles because of the vanishingly small values of $\partial B_z/\partial\rho$ in these regions. Values of $K_p$ are approximately 1/2 to 3/4 as large as those shown here for electrons.

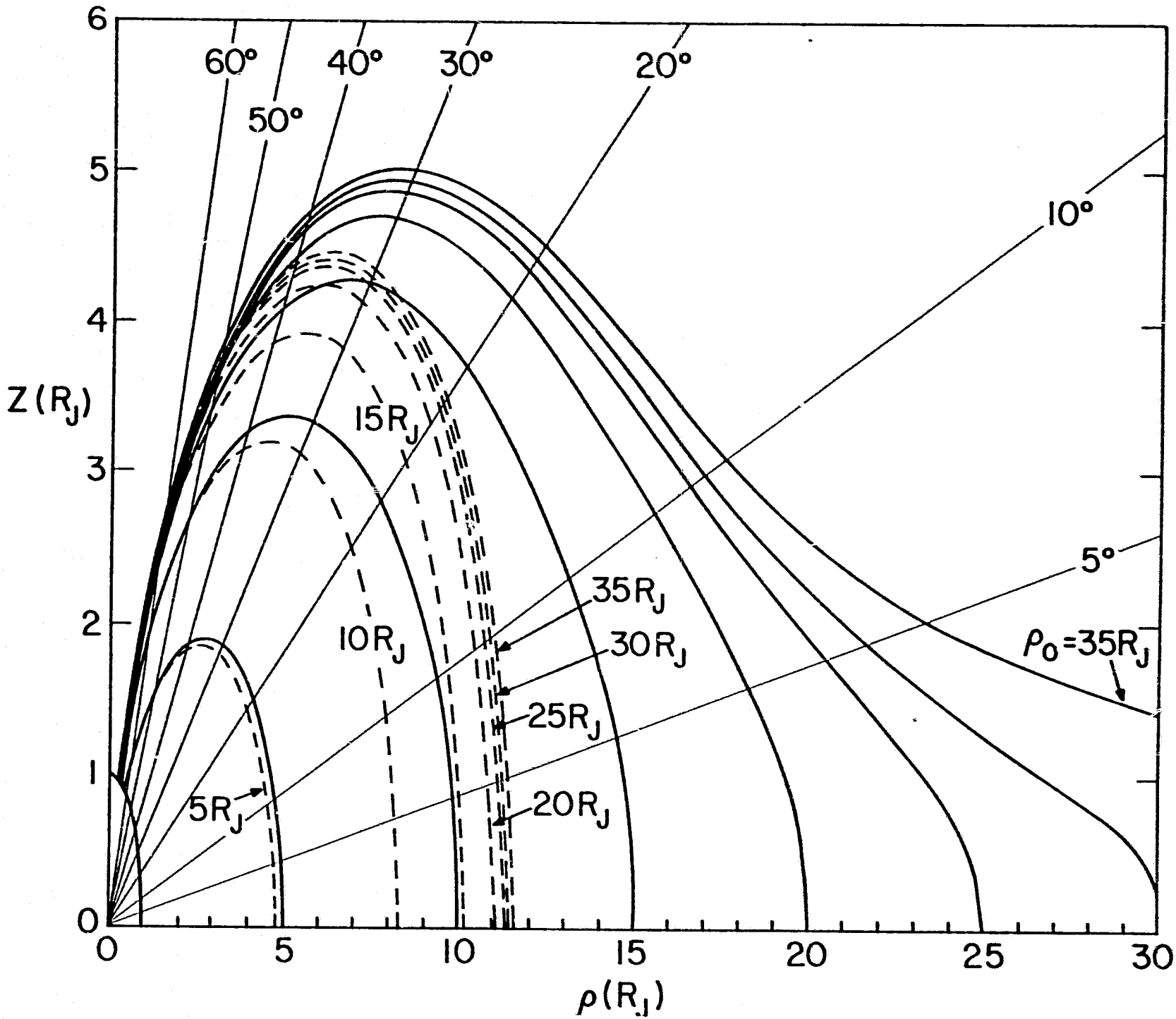
60°
50°
40°
30°
20°
10°
5°
15R_J
10R_J
5R_J
35R_J
30R_J
25R_J
20R_J
ρ_0=35R_J
Z(R_J)
ρ(R_J)
0
1
2
3
4
5
6
0
5
10
15
20
25
30

Figure 1a

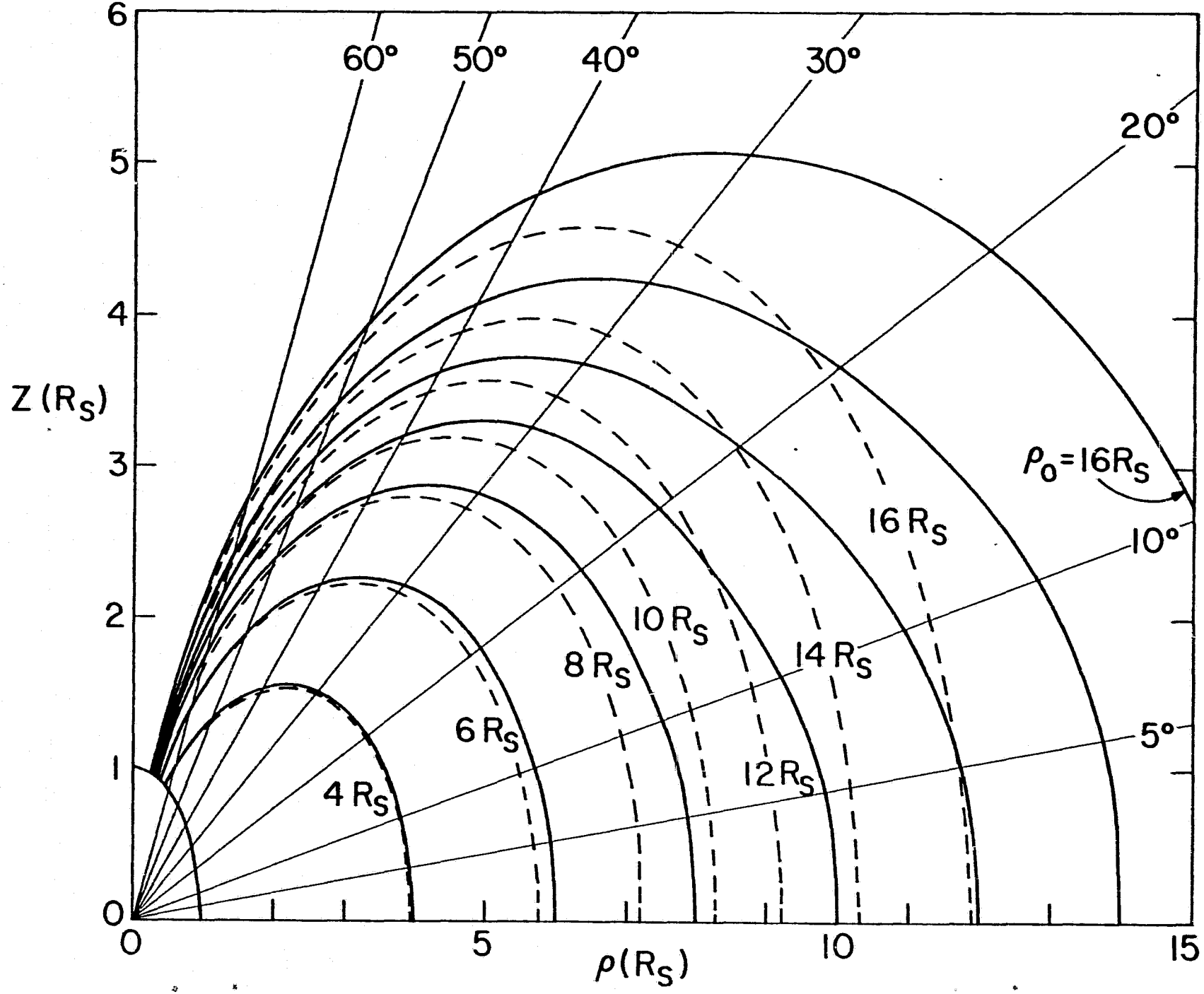
60°
50°
40°
30°
20°
10°
5°
$\rho_0 = 16 R_S$
16 $R_S$
14 $R_S$
12 $R_S$
10 $R_S$
8 $R_S$
6 $R_S$
4 $R_S$
Z ($R_S$)
$\rho$ ($R_S$)
0
1
2
3
4
5
6
0
5
10
15

Figure 1b

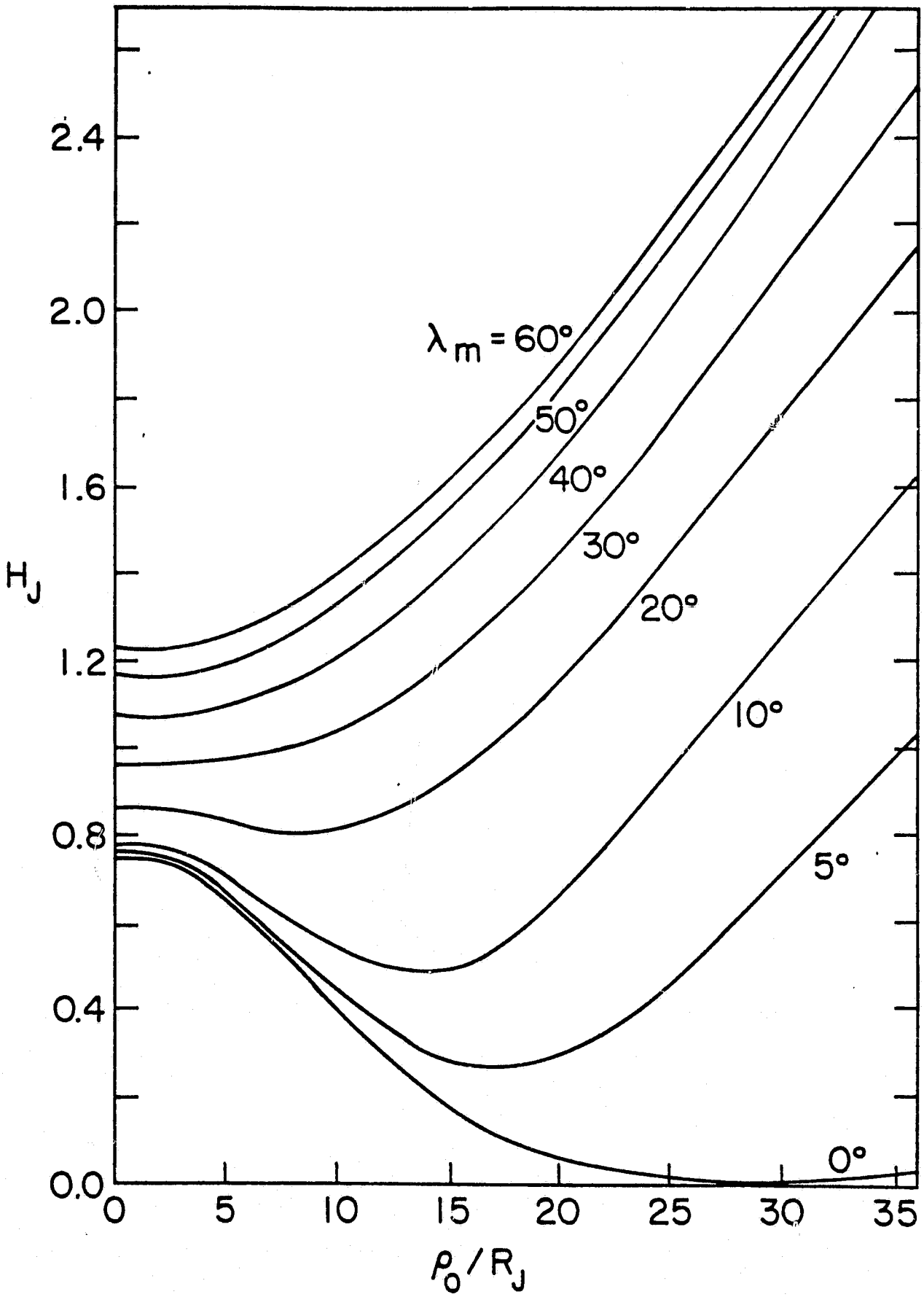
2.4
2.0
1.6
1.2
0.8
0.4
0.0
$H_J$
$\lambda_m = 60°$
50°
40°
30°
20°
10°
5°
0°
0
5
10
15
20
25
30
35
$\rho_0 / R_J$

Figure 2a

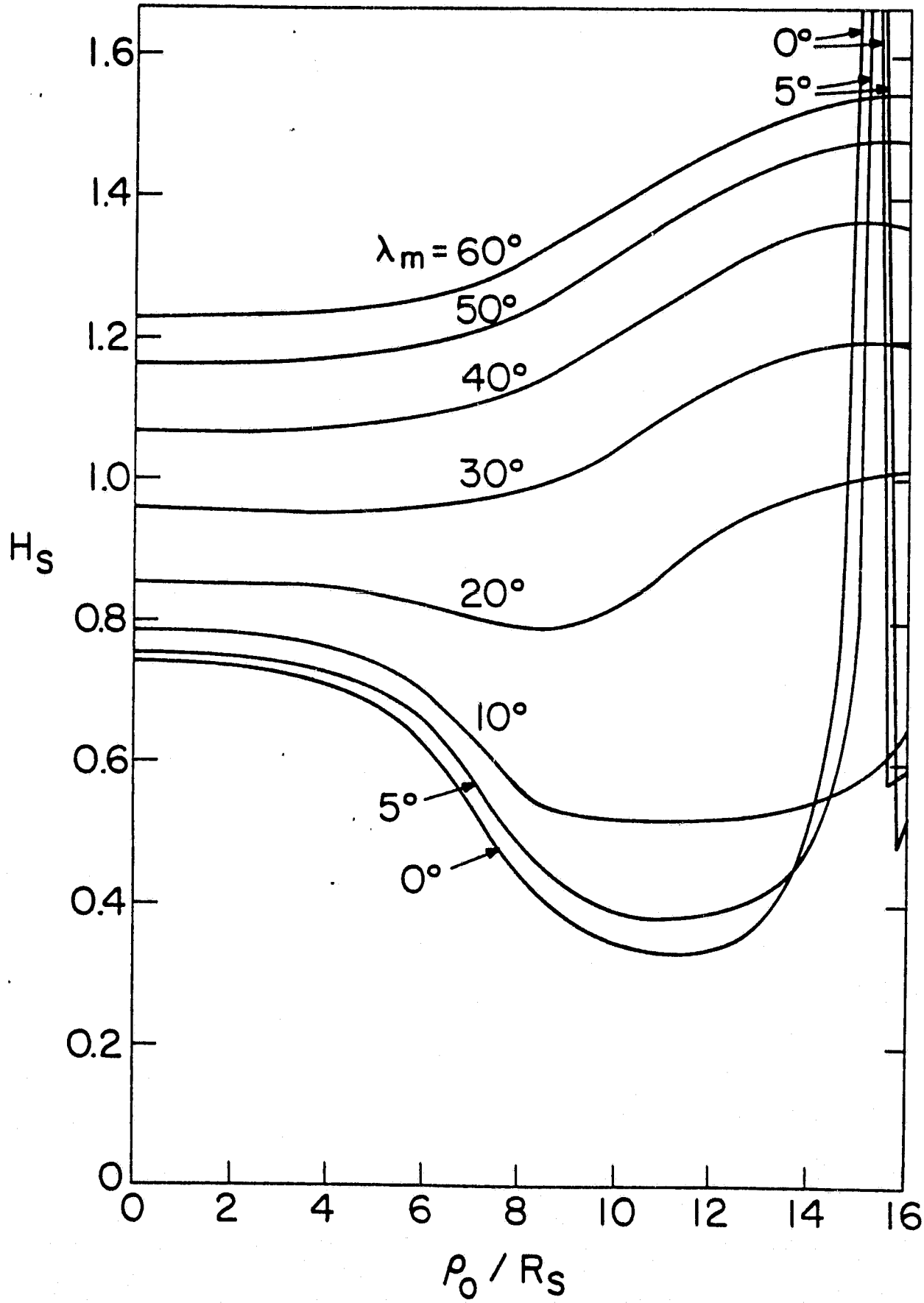
1.6
1.4
1.2
1.0
0.8
0.6
0.4
0.2
0
$H_S$
0°
5°
$\lambda_m = 60°$
50°
40°
30°
20°
10°
5°
0°
0
2
4
6
8
10
12
14
16
$\rho_0 / R_S$

Figure 2b

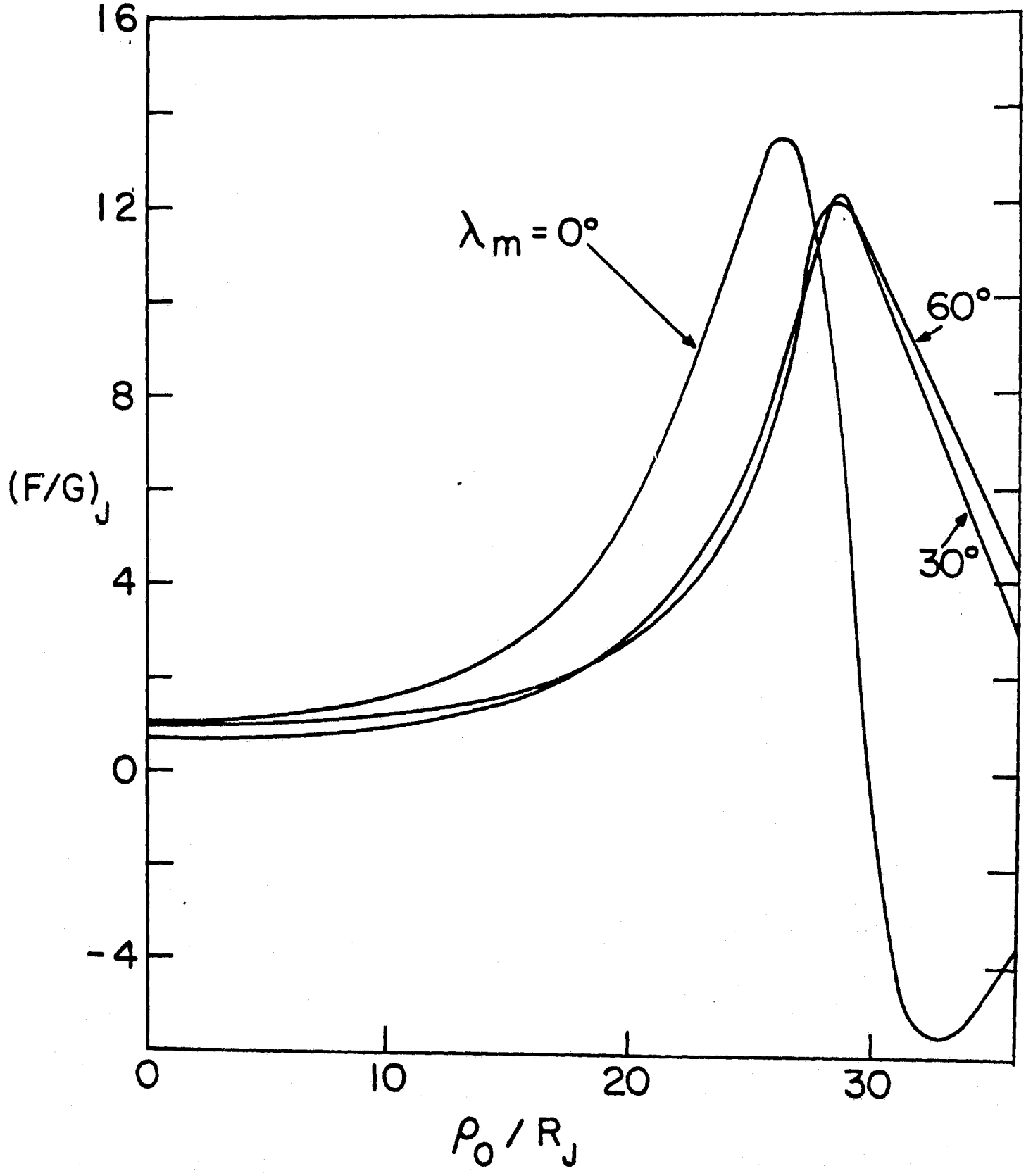


Figure 3a

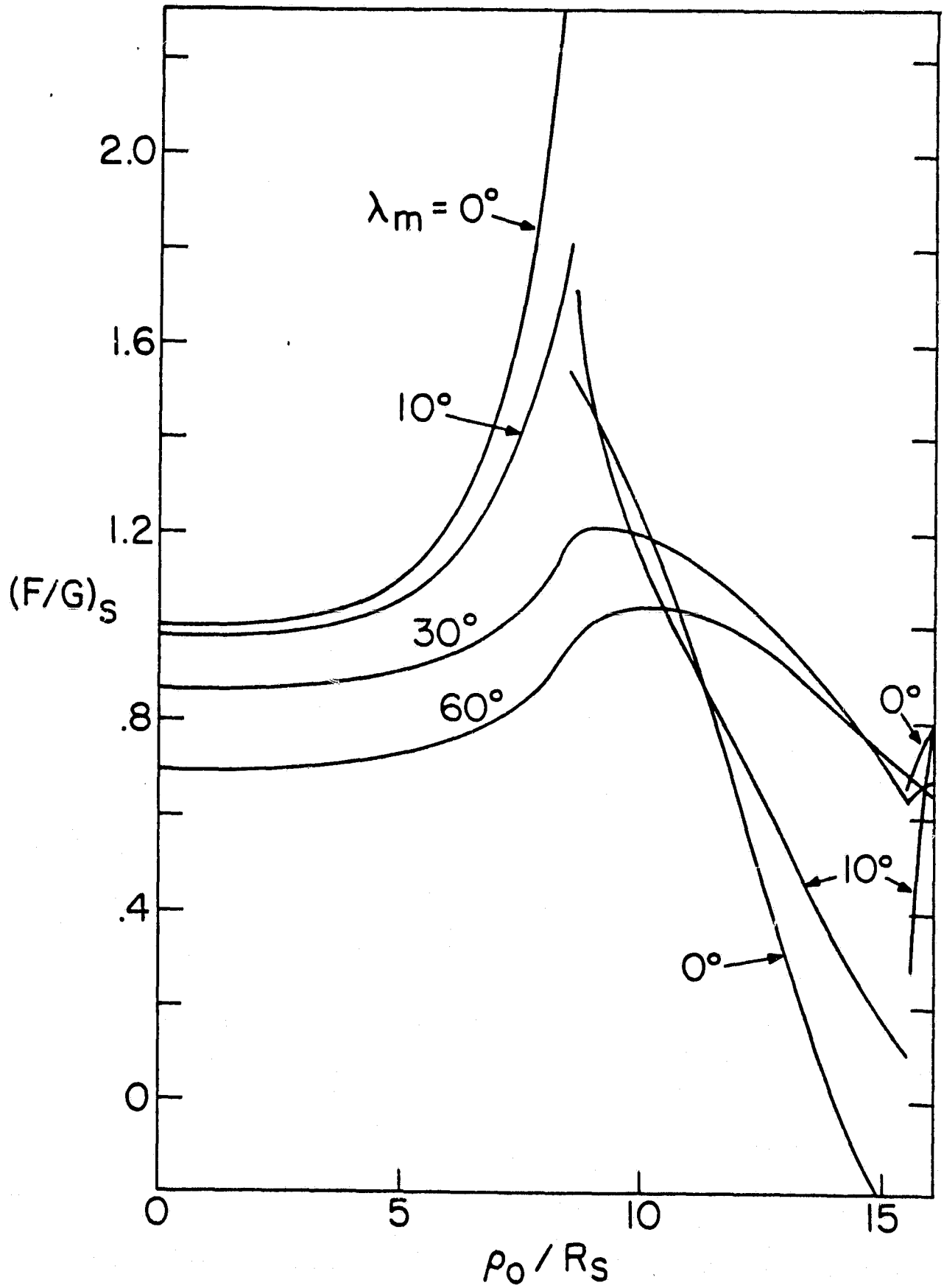


Figure 3b

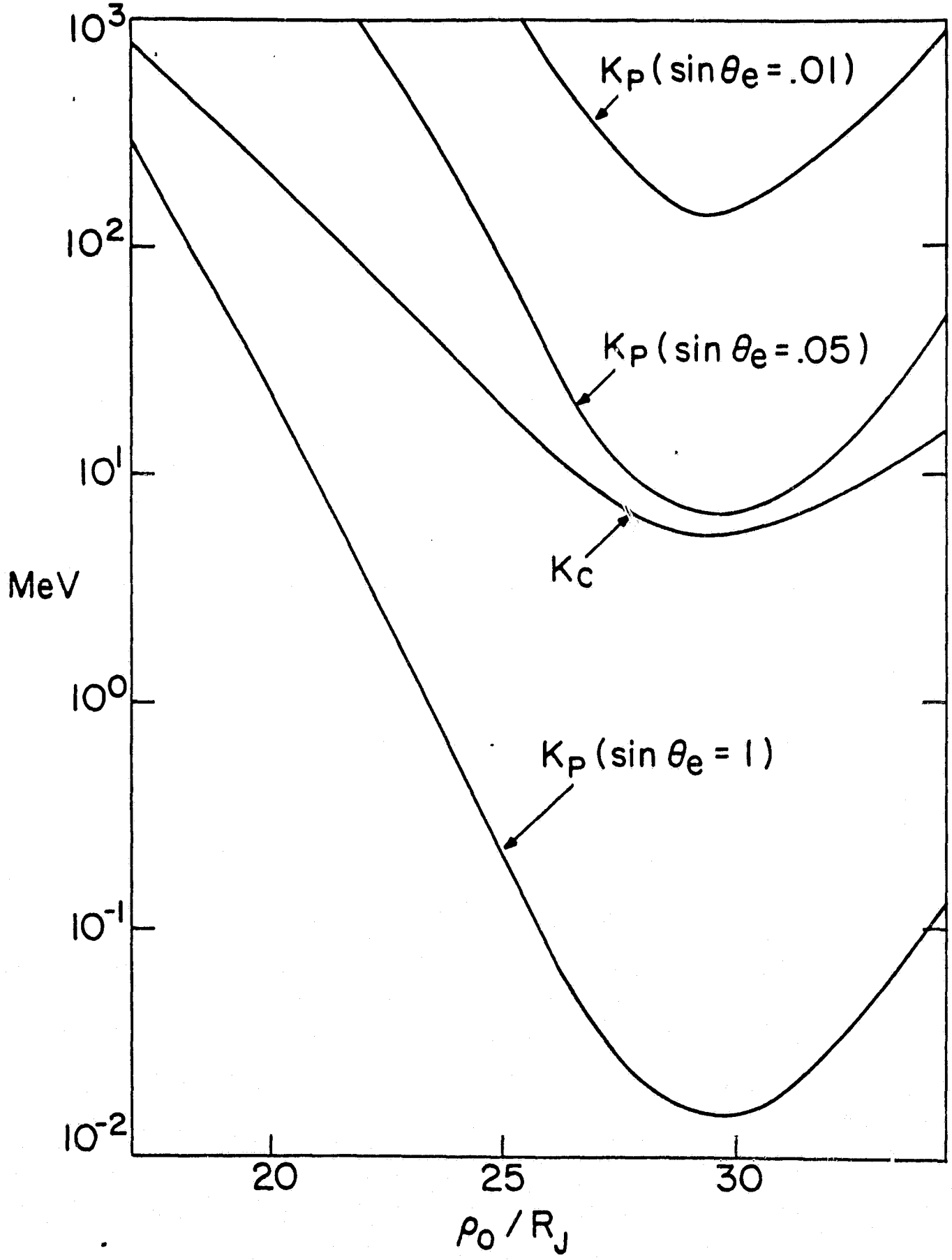
$10^3$
$10^2$
$10^1$
$10^0$
$10^{-1}$
$10^{-2}$
MeV
$K_P(\sin\theta_e = .01)$
$K_P(\sin\theta_e = .05)$
$K_C$
$K_P(\sin\theta_e = 1)$
20
25
30
$\rho_0 / R_J$

Figure 4a

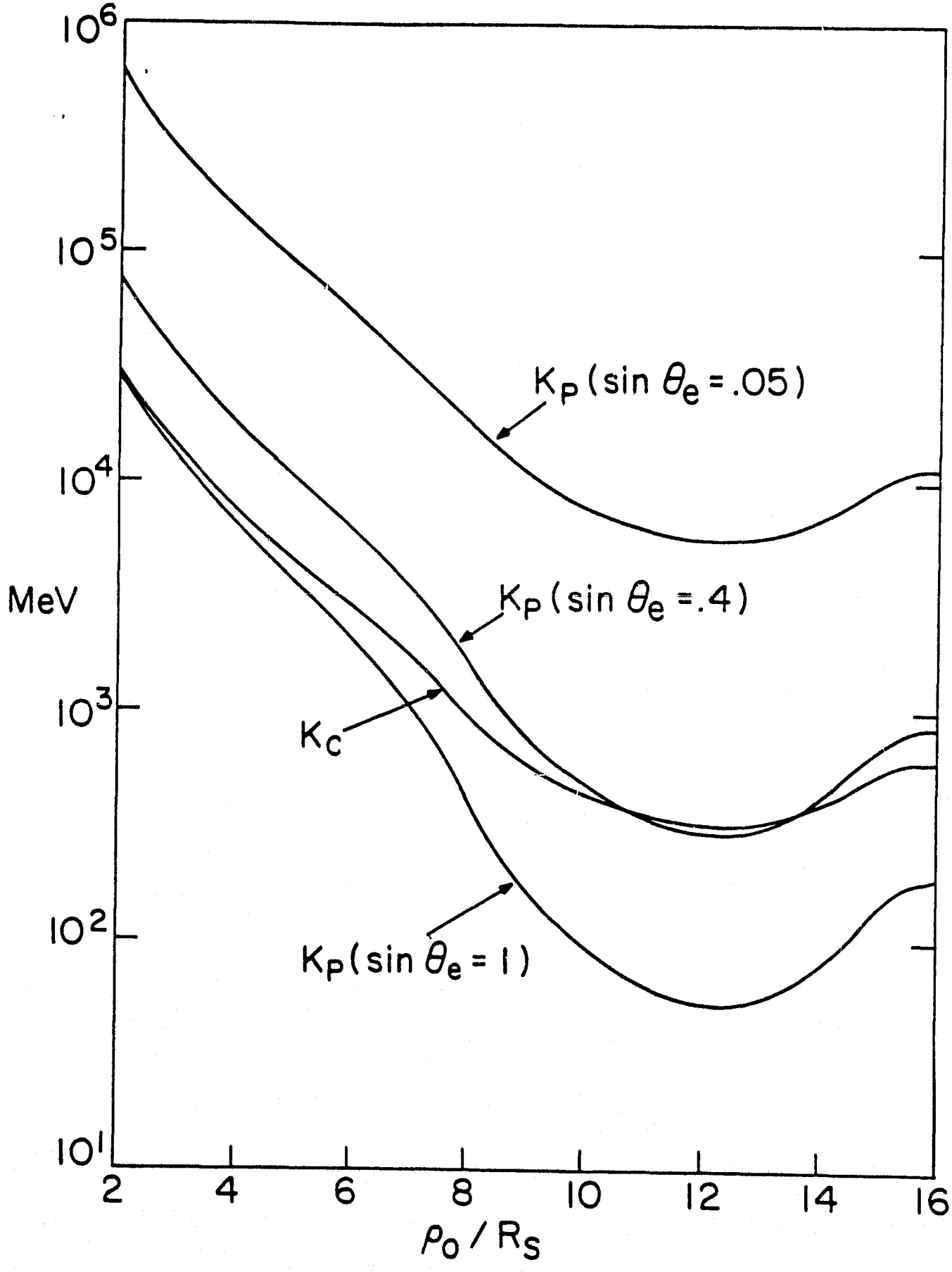
$10^6$
$10^5$
$10^4$
$10^3$
$10^2$
$10^1$
MeV
$K_P(\sin\theta_e = .05)$
$K_P(\sin\theta_e = .4)$
$K_C$
$K_P(\sin\theta_e = 1)$
2
4
6
8
10
12
14
16
$\rho_0 / R_S$

Figure 4b

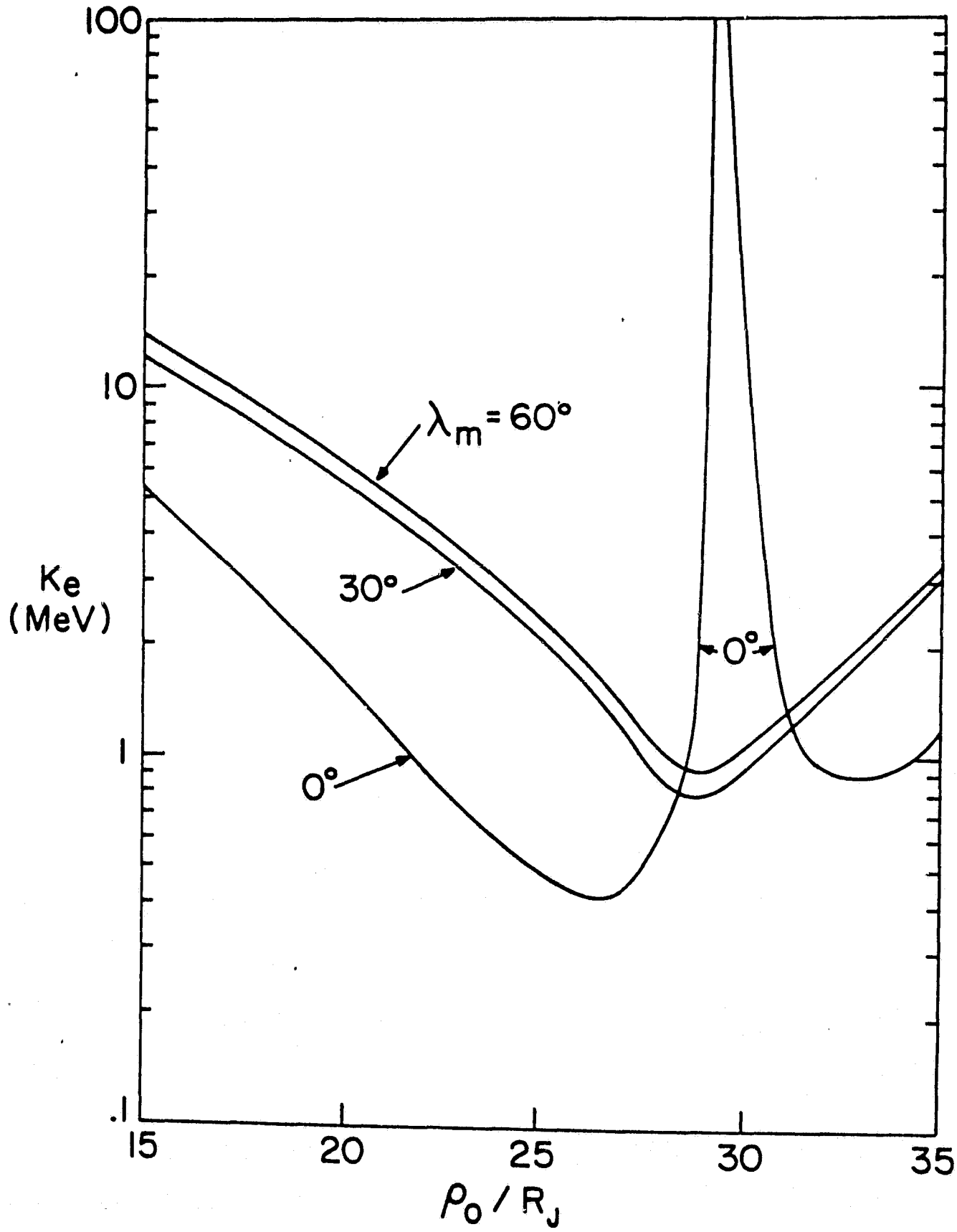


Figure 5a

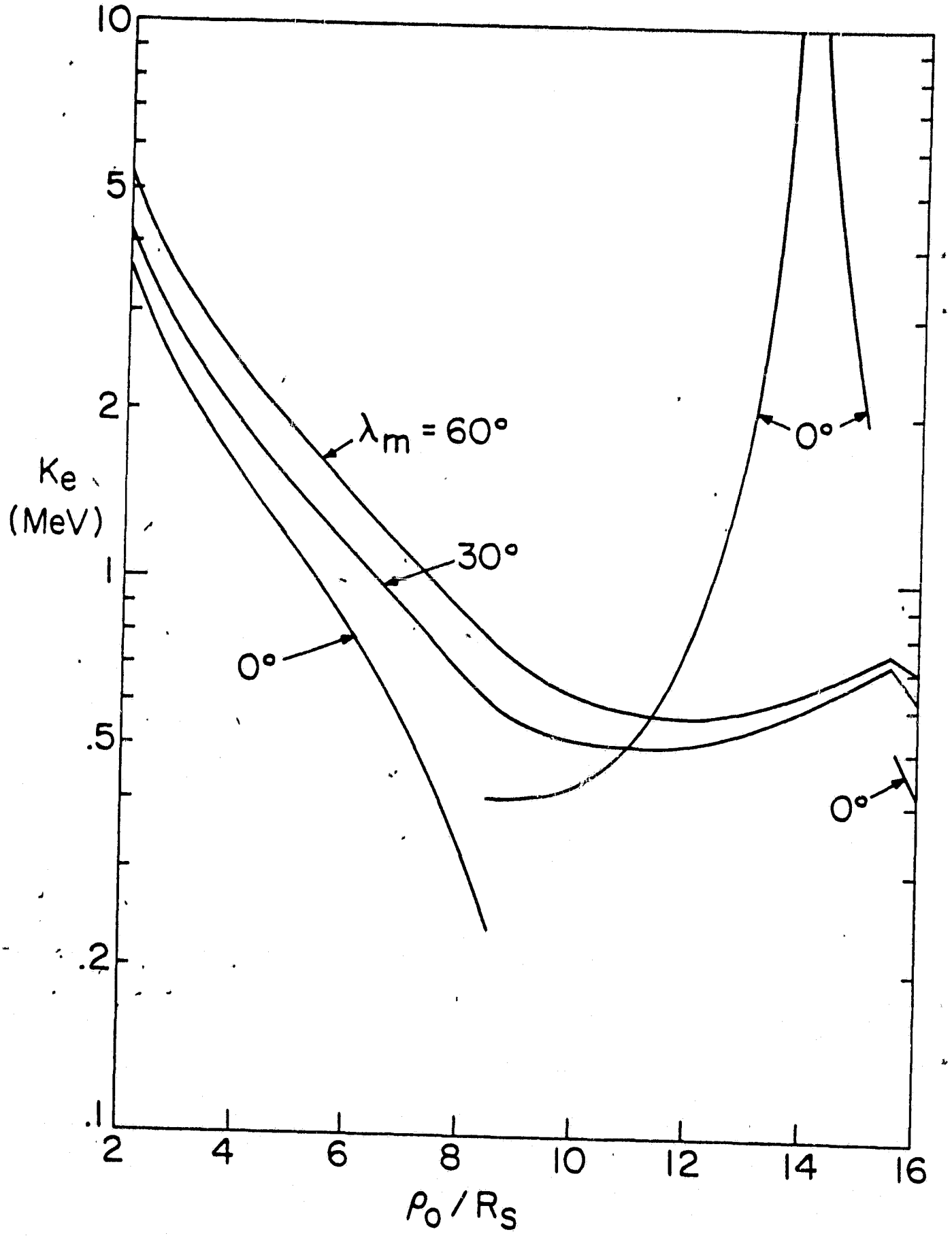


Figure 5b